

4. J.K. Park, H.S. An, and J.N. Lee, Design of the tree-shaped UWB antenna using fractal concept, *Microwave Opt Technol Lett* 50 (2008), 155–158.
5. R. Kumar, P. Malathi, and K. Sawant, On the design of wheel shaped fractal antenna, *Microwave Opt Technol Lett* 53 (2011), 155–158.
6. R. Ghatak, B. Biswas, A. Karmakar, and D.R. Poddar, A circular fractal UWB antenna based on descartes circle theorem with band rejection capability, *Prog Electromagn Res C* 37 (2013), 235–248.
7. A.R. Maza, B. Cook, G. Jabbour, and A. Shamim, Paper-based inkjet-printed ultra-wideband fractal antennas, *IET Microwave Antennas Propag* 6 (2012), 1366–1373.
8. Y.S. Li, X.D. Yang, C.Y. Liu, and T. Jiang, Analysis and investigation of a cantor set fractal UWB antenna with a notch-band characteristic, *Prog Electromagn Res B* 33 (2011), 99–114.
9. R. Kumar and P. Malathi, On the design of CPW-feed diamond shape fractal antenna for UWB applications, *Int J Electron* 98 (2011), 1157–1168.
10. D.D. Krishna, M. Gopikrishna, C.K. Aanandan, P. Mohanan, and K. Vasudevan, Compact wideband Koch fractal printed slot antenna, *IET Microwave Antennas Propag* 3 (2009), 782–789.
11. M.M. Islam, M.T. Islam, M. Samsuzzaman, M.R.I. Faruque, and N. Misran, Microstrip line-fed fractal antenna with a high fidelity factor for Uwb imaging applications, *Microwave Opt Technol Lett* 57 (2015), 2580–2585.
12. K.K. Sawant and C.R.S. Kumar, CPW fed hexagonal micro strip fractal antenna for UWB wireless communications, *Int J Electron Commun (AEÜ)* 69 (2015), 31–38.
13. Ansoft Corporation, HFSS, High frequency structure simulator ver. 11, finite element package. Available at: <http://www.ansoft.com>.
14. CST Inc, CST Microwave Studio Suite 2011. (2007).
15. S. Singhal and A.K. Singh, Crescent shaped dipole antenna for ultra wideband applications, *Microwave Opt Technol Lett* 57 (2015), 1773–1782.
16. R.V.S.R. Krishna and R. Kumar, Asymmetrically fed slotted rectangular monopole antenna for dual polarization, *Microwave Opt Technol Lett* 55 (2013), 2160–2165.
17. M.J. Ammann and Z.N. Chen, An asymmetrical feed arrangement for improved impedance bandwidth of planar monopole antennas, *Microwave Opt Technol Lett* 40 (2004), 156–158.
18. C. A. Balanis, *Antenna theory: Analysis and design*, 3rd ed., Wiley, India Edition, 2012
19. W. Weisbeck, G. Adamiuk, and C. Sturm, Basic properties and design principles of UWB antennas, *Proc IEEE* 97 (2009), 372–385.
20. W. Sorgel and W. Weisbeck, Influence of the antennas on the ultra-wideband transmission, *EURASIP J Appl Signal Process* 3 (2005), 296–305.
21. Electronic Communications Committee (ECC), “The European table of Frequency Allocations and Applications,” ERC Report 25, 2014.

© 2016 Wiley Periodicals, Inc.

RCS BASED TARGET RECOGNITION WITH REAL FMCW RADAR IMPLEMENTATION

Yoonjin Lee,¹ Hosung Choo,² Soojin Kim,³ and Hongseok Kim¹

¹Department of Electronic Engineering, Sogang University, Korea; Corresponding author: hongseok@sogang.ac.kr

²School of Electronic and Electrical Engineering, Hongik University, Seoul, Korea

³Agency for Defense Development, Daejeon, Korea

Received 10 November 2015

ABSTRACT: In this article, we investigate the methods that can realize automatic target recognition and tracking by exploiting signal distribution of radar cross section (RCS) with frequency modulated continuous

wave (FMCW) radar. In doing this we use the real RCS data measured from the short-range FMCW vehicle radar. We estimate the continuous valued degree of freedom and the mean of RCS distribution using maximum likelihood estimation (MLE) assuming that RCS follows gamma distribution. The experiments with real radar verify that parameterized gamma distributions for three targets of man, vehicle, and drone closely follow the empirical distributions. Then, we apply maximum a posteriori criterion (MAP) for target recognition. The average recognition probabilities for man, vehicle, and drone using MAP are 85%, 100%, and 92%, respectively. Since the vehicle has distinct RCS and thus perfectly recognizable, we apply a support vector machine (SVM) hoping to better classify the man and the drone. The man is recognized with similar accuracy, but the drone is not due to the lack of training samples, of which constraint is imposed by real implementation and experiment. © 2016 Wiley Periodicals, Inc. *Microwave Opt Technol Lett* 58:1745–1750, 2016; View this article online at wileyonlinelibrary.com. DOI 10.1002/mop.29901

Key words: FMCW short-range radar; target recognition; RCS; KS-distance; maximum-likelihood

1. INTRODUCTION

Radar has been used to recognize targets and to estimate the distance from the target by analyzing reflected radar signal. Research on radar has been mainly for military when it is needed to notify the location of enemy flights or vessels from a long distance [1,2]. Previous research of target recognition took advantage of radar cross section (RCS) values reflected from the target. In doing this, Swerling made a statistical model based on chi-square distribution [3] to discern objects, typically either airplanes or ships depending on the degree of freedom, which is, either 2 or 4, respectively. In this regard, RCS values have been usually measured by a long-range pulsed radar. Recently, however, radar is used for other than military purposes; for example, short-range radar is located on the front or the rear of autonomous unmanned vehicles to detect, recognize, track, or dodge targets. Since frequency modulated continuous wave (FMCW) is simpler than other radar systems, it is easier to apply additional techniques such as digital beamforming [4]. Accordingly, it becomes important to analyze signal from short-range FMCW radar for target recognition [5,6].

In this article, we investigate several target recognition methods. Assuming that RCS distribution follows gamma distribution that is a generalized version of chi-square distribution [7], we estimate the continuous valued parameters that specify the RCS

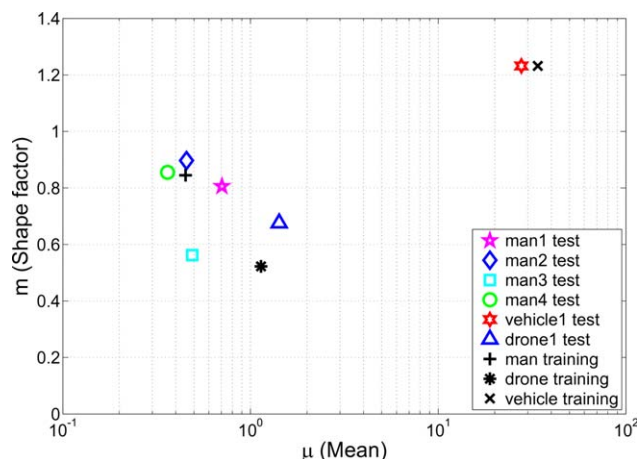


Figure 1 Shape factor and mean plot. [Color figure can be viewed in the online issue, which is available at wileyonlinelibrary.com]

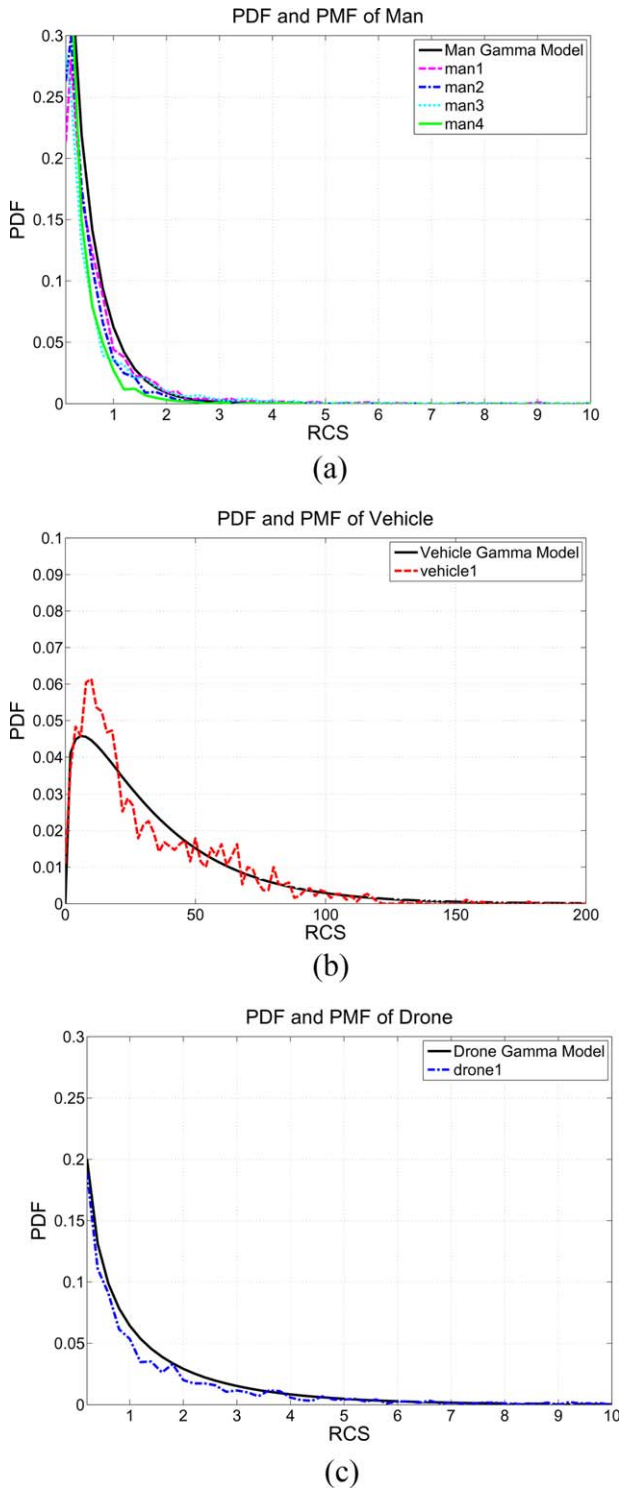


Figure 2 (a) RCS of man: empirical distribution (dashed line) and estimated distribution (solid line); (b) RCS of vehicle: empirical distribution (dashed line) and estimated distribution (solid line); (c) RCS of drone: empirical distribution (dashed line) and estimated distribution (solid line). [Color figure can be viewed in the online issue, which is available at wileyonlinelibrary.com]

distribution using the maximum likelihood estimation (MLE). Then we first apply Kolmogorov-Smirnov (KS) distance for target recognition but find KS distance not effective in discerning man and drone since their distributions are similar. Hence, we apply maximum *a posteriori* (MAP) criterion for target recognition and

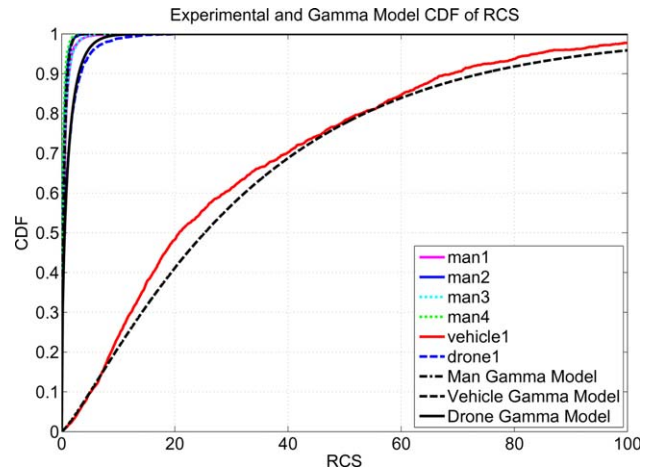


Figure 3 CDF of empirical and estimated RCS. [Color figure can be viewed in the online issue, which is available at wileyonlinelibrary.com]

compute the probability that the unknown target would be a specific object. Our results show that MAP is good for recognizing man, drone, and vehicle while a support vector machine (SVM) may not work well under the limited number of training samples.

This paper is organized as follows. In Section 2, we present gamma distribution for RCS modeling. In Section 3, the parameter estimation with MLE is derived and target recognition methods based on MAP and SVM are presented, respectively. The experiments and analysis of measured data are followed in Section 4, and the conclusion is provided in Section 5.

2. RCS DISTRIBUTION MODEL

RCS can represent the characteristics of target surface; the radar receives the same reflective force coming out from the target when the energy is equally distributed on the target's surface. The RCS σ of the target is defined as

$$\sigma = \lim_{R \rightarrow \infty} 4\pi R^2 \frac{|E_s|^2}{|E_0|^2} \quad (1)$$

where R is the distance between radar and target, E_s is the spreading intensity reflected from the target, and E_0 is the spreading intensity exposed to the target from radar. Traditional common targets are airplanes, vehicles, vessels, and grounds. Typically, RCS value is roughly proportional to the size of the target. In this study, however, targets are similar in size when seen by radar, and also significantly smaller than traditional targets, which makes target recognition challenging.

RCS is typically modeled by chi-square distribution (Swelling model 1–4), log-normal distribution, gamma distribution, etc. Among these, we assume that the distributions of our targets (man, drone, and vehicle) follow gamma distribution with parameter $\theta = (\mu, m)$,

$$P(x|\theta) = \frac{m}{(m-1)! \mu} \left(\frac{mx}{\mu}\right)^{m-1} \exp\left(-\frac{mx}{\mu}\right) \quad (2)$$

where μ is the mean and m is the shape factor. Note that $2m$ is so called the degree of freedom. Specifically, Swerling model discerns targets based on the degree of freedom, e.g., 2 for airplanes and 4 for ships using chi-square distribution, which is a special case of gamma distribution.

TABLE 1 KS-Distance Between Test Data and Training Data

Test burst	Training by man			Training by vehicle			Training by drone		
	Test date type			Test date type			Test date type		
	Man-1	Vehicle-1	Drone-1	Man-1	Vehicle-1	Drone-1	Man-1	Vehicle-1	Drone-1
1	0.272	0.974	0.366	0.947	0.489	0.842	0.193	0.916	0.193
2	0.131	0.958	0.195	1.000	0.380	1.000	0.211	0.907	0.151
3	0.151	0.937	0.185	0.992	0.626	0.991	0.261	0.928	0.261
4	0.443	0.889	0.252	1.000	0.512	0.989	0.371	0.838	0.155
5	0.370	0.970	0.420	0.883	0.567	0.720	0.480	0.789	0.260
6	0.139	0.928	0.147	0.930	0.262	0.836	0.408	0.822	0.180
7	0.286	0.974	0.408	0.975	0.361	0.941	0.199	0.915	0.128
8	0.216	0.872	0.084	0.955	0.430	0.877	0.168	0.915	0.168

3. TARGET RECOGNITION

3.1. Parameter Estimation of RCS Distribution Using MLE
 Given the measured RCS vector $\mathbf{x}=(x_1, x_2, \dots, x_d)$ where d is the number of chirps in a single burst, we estimate $\Theta=(\theta_1, \dots, \theta_d)$ using MLE. To find out Θ that maximizes the likelihood $P(\mathbf{x}|\Theta)$ or its log-likelihood $\log P(\mathbf{x}|\Theta)$ given \mathbf{x} , we assume that x_i is an independent random variable [8], and the likelihood function of \mathbf{x} with Θ is given by

$$P(\mathbf{x}|\Theta) = \prod_{i=1}^d \frac{m_i}{(m_i-1)! \mu_i} \left(\frac{m_i x_i}{\mu_i}\right)^{m_i-1} \exp\left(-\frac{m_i x_i}{\mu_i}\right) \quad (3)$$

Then, we find Θ that maximizes the log likelihood,

$$L(\Theta) = \log P(\mathbf{x}|\Theta) \quad (4)$$

Since one burst is very short, it is reasonable to assume that the statistics of RCS does not change in a burst, i.e., $x_i, i=1, \dots, d$ are identically distributed, and thus we assume $\theta_i=\theta$ for all i . Then, by taking the derivative of L with respect to μ , we find μ that satisfies $\frac{\partial L}{\partial \mu}=0$. As one might expect, μ turns out to be the average RCS of the burst, i.e.,

$$\mu = \frac{1}{d} \sum_{i=1}^d x_i \quad (5)$$

Similarly, we find m that satisfies $\frac{\partial L}{\partial m}=0$. Due to space limitation, we omit the derivation, but one can show that m is the solution of the following equation,

$$v(m) = -\frac{1}{d} \sum_{i=1}^d \log\left(\frac{x_i}{\mu}\right) \quad (6)$$

where $v(m) = \log(m) - \frac{\partial}{\partial m} \log \Gamma(m)$ and $\Gamma(m)$ is the gamma function. Then, Eq. (6) needs be numerically solved using root-finding algorithms, e.g., the bisection method.

TABLE 2 The Target Recognition Result With KS-Distance

Test target	Training by man	Training by vehicle	Training by drone
Man-1	75%	0%	25%
Man-2	93.75%	0%	6.25%
Man-3	37.5%	0%	62.5%
Man-4	100%	0%	0%
Vehicle-1	0%	0%	0%
Drone-1	18.75%	0%	81.25%

3.2. Target Recognition Using MAP Criterion

Next step is to recognize unknown target given \mathbf{x} . In doing this we take a probabilistic approach. That is, instead of asserting what the target is, we compute the probability that \mathbf{x} corresponds to some specific target. It can be done by using MAP criterion. Let $j \in \mathfrak{J}$ denote a target and \mathfrak{J} denote a collection of all known targets. Using Bayes' rule, the probability that \mathbf{x} would be a target j is computed by

$$P(\theta_j|\mathbf{x}) = \frac{P(\mathbf{x}|\theta_j)P(\theta_j)}{p(\mathbf{x})} \quad (7)$$

Note that $P(\theta_j)$ is a priori probability that a target j would appear, which can be learned during online operation. In case $P(\theta_j)$ is unknown, it is reasonable to assume that each target appears equally likely, which makes the MAP probability simply the normalized likelihood

$$P(\theta_j|\mathbf{x}) = \frac{P(\mathbf{x}|\theta_j)}{\sum_j P(\mathbf{x}|\theta_j)} \quad (8)$$

In this case, MAP-based target recognition boils down to maximum likelihood (ML) based target recognition except that it gives target probability rather than asserting the target. Finally, the unknown target is declared as $j^* = \arg \max_{j \in \mathfrak{J}} P(\theta_j|\mathbf{x})$ with probability $P(\theta_{j^*}|\mathbf{x})$.

3.3. Target Classification Using Support Vector Machine (SVM)

In addition to MAP, we also apply SVM to classify targets based on training data. Let \mathbf{x}_k and $y_k, k=1, \dots, M$ denote training RCS vectors and the corresponding target types. Then, using SVM, which is a supervised learning technique, we find the hyperplane \mathbf{w} that separates objects into two groups (i.e., either labeled $y_k=1$ or -1) while maximizing the distance between the closest \mathbf{x}_k and the hyperplane:

$$\min \frac{1}{2} \mathbf{w}^T \mathbf{w} \quad (9)$$

$$s.t. \ y_k(\mathbf{w}^T \mathbf{x}_k + b) \geq 0, \text{ for } k=1, \dots, M \quad (10)$$

where \mathbf{w} is the normal vector of the hyperplane, $\mathbf{w}^T \mathbf{x} + b = 0$, b is the bias term where $|\mathbf{w}^T \mathbf{x} + b| = 1$, and M is the number of training vectors. In doing this, we use a kernel function $\Phi(x)$ to perform a non-linear classification, i.e., \mathbf{x}_k is replaced by $\Phi(\mathbf{x}_k)$ in Eq. (10).

4. EXPERIMENTAL RESULTS WITH REAL FMCW RADAR

4.1. Experiment Setup

Unlike traditional electromagnetic simulation-based approach, we perform experiments with real FMCW radar implementation

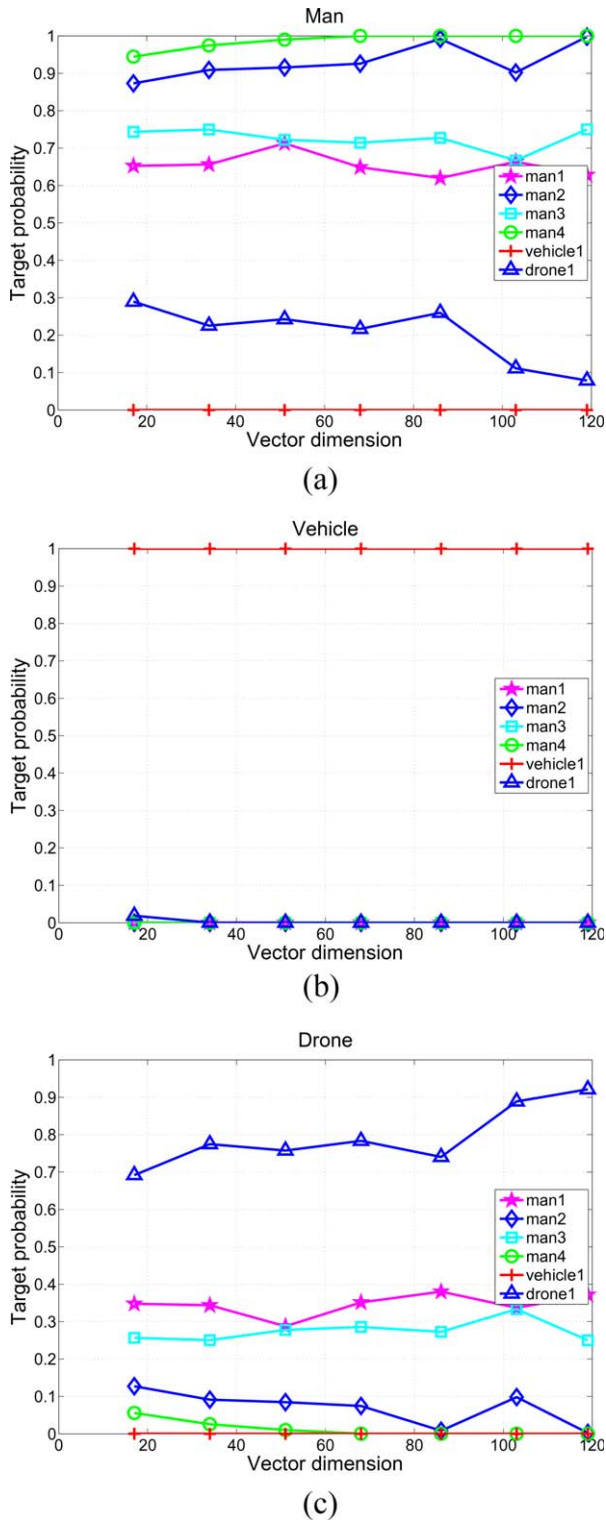


Figure 4 (a) Probability of man: Target probabilities for various input vectors of man-1,2,3,4, drone-1, and vehicle-1; (b) Probability of vehicle: Target probabilities for various input vectors of man-1,2,3,4, drone-1, and vehicle-1; (c) Probability of drone: Target probabilities for various input vectors of man-1,2,3,4, drone-1, and vehicle-1. [Color figure can be viewed in the online issue, which is available at wileyonlinelibrary.com]

using parabolic antenna with the operating frequency at 76.4–76.6 GHz. Detailed radar specification is as follows. The bandwidth of waveform, B_{FM} is 200 MHz, the number of range bins, N_{FFT} is 256, the number of chirps per one burst, N_{chirp} is 119,

and the duration of one chirp, T is 33 μ sec. One of the advantages of FMCW radar is its inherent capability of computing the distance as well as the speed of moving object by applying 2-dimensional fast Fourier transform (FFT) of the FMCW beat frequency [9]. However, in processing FFT, main lobe that obtains the received target signal is not significantly distinguished with side lobe, and thus we reduce the side lobe and amplify the main lobe by applying Hanning window [10]. Then 1-d FFT is performed to obtain the distance from the target [11].

Our targets in experiments are man, drone, and vehicle. Each target moves slowly around within the distance from 5 to 10 m from the radar. Based on the radar specification, one burst of RCS vector x has 119 chirps, and thus the maximum of d is 119. We measure totally 16 bursts. Due to the radar hardware processing time, the total number of bursts is limited by 16 in this experiment. Note that one chirp generates one RCS value, and thus, totally we have $119 \times 16 = 1904$ RCS values per target. We use the first half (952 RCS values) as a training set for estimating parameter θ when using MAP and for constructing support vectors when using SVM, respectively. The test sets are made from the second half of RCS values.

4.2. Results

4.2.1. RCS Parameters Estimated by MLE. We have four scenarios for the target of man. The case of man-1 is when a person walks without swinging arms. The case of man-2 is when he walks through swinging arms widely. The case of man-3 is when he runs. The case of man-4 is when he walks while rotating. We have a single scenario for vehicle and drone, respectively. The estimated parameters $\theta = (\mu, m)$ for the targets are shown in Figure 1. The estimated mean, μ , from man training data is 0.451, from vehicle training data is 33.90, and from drone training data is 1.138. The value of estimated shape factor, m , from man training data is 0.845, from vehicle training data is 1.232, and from drone training data is 0.522. As can be seen, the vehicle has quite distinct RCS mean μ and the shape factor m , which makes it easy to discern the vehicle from others. By contrast, the man and the drone have similar values of μ and m , which makes target recognition challenging.

4.2.2. RCS Distribution. Figure 2 shows the empirical RCS distributions (dashed line) and its estimation by gamma distributions (solid line) for man, vehicle, and drone, respectively. We see that gamma distribution closely follows the measured distributions for all three types of targets. Figure 3 shows the measured cumulative density functions (CDFs) of three targets (dashed line) and its estimated CDF (solid line). We also see that the estimated distributions closely follow the empirical CDFs. To quantify the distribution estimation accuracy we compute the KS-distance between the empirical and estimated distributions. The KS-distance d_{KS} for two CDFs $F(x)$ and $G(x)$ is defined as $d_{KS} = \max_x |F(x) - G(x)|$. Tables 1 and [2] show the result. One may think that targets can be recognized using KS-distance. To explore the possibility we cross-compare the KS-distances of all possible pairs of the estimated distributions obtained from training sets and empirical distributions obtained from each burst in test sets. Table 1 shows one example of the calculated KS-distance between trained data's estimated probability density function (PDF) and test data's empirical probability mass function (PMF). Table 2 is the result of target classification accuracy using KS-distance. As shown in Table 2, it is hard to use KS-distance to reliably recognize the target; for example, man-3 is miss-classified as a drone with 62.5%.

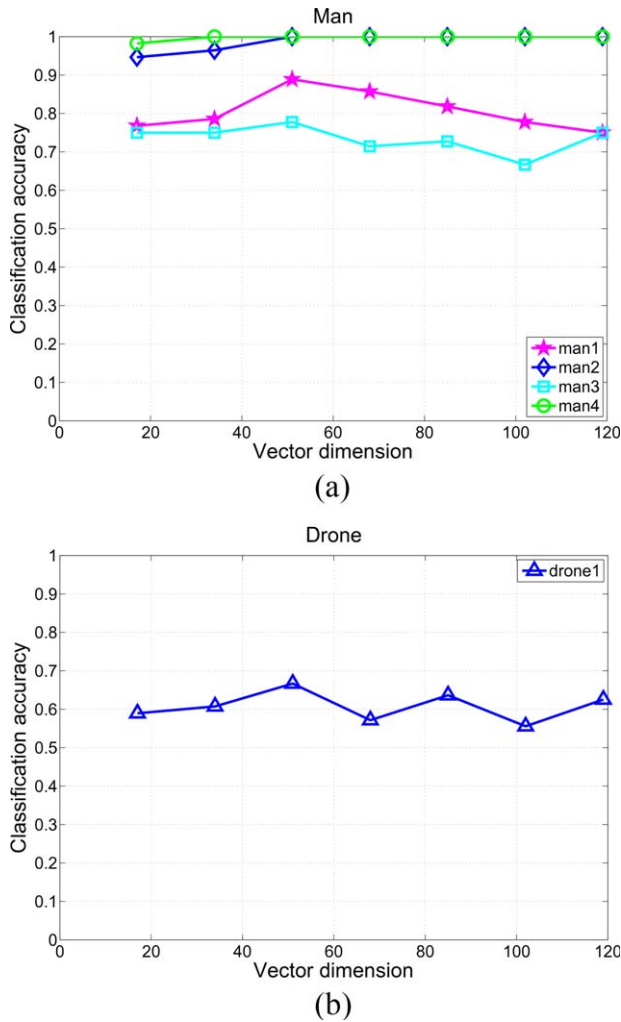


Figure 5 (a) Man: Classification accuracy using SVM; (b) Drone: Classification accuracy using SVM. [Color figure can be viewed in the online issue, which is available at wileyonlinelibrary.com]

4.2.3. MAP Based Target Recognition. Now we use MAP for target recognition as explained in Section 3.2. Since \mathbf{x} is either from man-1, 2, 3, 4, vehicle or drone, we calculate $P(\theta_j|\mathbf{x})$ for each $j \in \mathfrak{I}$ for six different test vectors \mathbf{x} . In doing this, to investigate the appropriate dimension of input vector \mathbf{x} , we also vary d , i.e., the size of \mathbf{x} from 17 to 119. Figure 4(a) shows the probability that the input vector \mathbf{x} would be a man. We see that man-2 and man-4 exhibits nearly 100% recognition probability when using one total burst as an input vector, which verifies that the radar hardware design of 119 chirps per burst is well chosen. However, as expected from Figure 1 and Table 2 where the distribution of man-1 and man-3 are deviated from the typical man case, man-1 and man-3 do not exhibit high recognition probabilities. We find the reason from inaccurate distance estimation for man-1 and man-3, which may come from imperfect FMCW radar implementation and hardware processing. The estimated speeds of man-1 and man-3 are unreasonably high, which implies that the distance estimation is not accurate. We expect that when new FMCW radar is developed, distance inaccuracy shall be improved. Figure 4(b) shows the probability that the input vector \mathbf{x} would be a vehicle. Perhaps it is not surprising to see that vehicle is recognized 100% even with a small d , e.g., 17. Figure 4(c) shows the probability that the input vector \mathbf{x}

would be a drone. We see that the drone can be recognized with more than 90% probability when full one burst is used.

4.2.4. SVM Based Target Recognition. We further extend our experiment using SVM. In applying SVM for target recognition, we investigate several types of kernel functions including linear, polynomial, and radial basis functions (RBF). Since the field-measured RCS for training set is limited, sophisticated kernel functions may have an overfitting problem. We find that the RBF kernel function is a good fit. When using the RBF kernel function, we also apply 10-fold cross validation. Note that unlike MAP, SVM only classifies the targets, and thus we compute the classification accuracy, not the target probability, by counting the number of correct classifications. In addition, even though there are three types of targets, we only apply SVM to discern the man and the drone because the vehicle is so distinctive. The training data and test data are same as MAP. The result of SVM is shown in Figure 5. As can be seen, classification accuracy of man is similar to the result of MAP. However, the result of drone, as seen in Figure 5(b), is not as good as that of MAP. The reason may come from that input vector dimension is high while the number of training samples is not sufficient.

5. CONCLUSION

In this article, we investigated methods for target recognition with real target RCS data measured in the field and extracted from short range FMCW radar hardware. We applied MLE to estimate the parameters of the empirical distribution of target RCS assuming gamma distribution. We calculated the KS-distance between estimated distribution and empirical distribution and verified that gamma distribution well captures the empirical RCS distribution. Then, we applied the MAP criterion for target recognition and found that MAP can effectively recognize targets in the real field with high probability, e.g., 85%, 100%, and 92% for man, vehicle, and drone, respectively. In addition, we applied SVM for separating the man and the drone and found that MAP shows better performance than SVM in the lack of the training samples. This is our initial work with real FMCW radar, and the future plan is to perform extended experiments when a new version of array-based FMCW radar hardware is developed with shorter processing time so that more RCS data are obtainable.

ACKNOWLEDGMENT

This research was supported by the Agency for Defense Development, Korea, under the contract UD130074ID.

REFERENCES

1. M.I. Skolnik, *RADAR handbook*, 3rd ed., McGraw-Hill, New York, 2008.
2. M.I. Skolnik, *Introduction to radar systems*, 3rd ed., McGraw-Hill, New York, 2001.
3. P. Swerling, Probability of detection for fluctuating targets, *IRE Trans Info Theory* 6 (1960), 269–308.
4. K.-T. Kim, Efficient radar target recognition using the MUSIC algorithm and invariant features, *IEEE Trans Antennas Propag* 50 (2002), 325–337.
5. S. Weiqiang, Radar cross section (RCS) statistical characterization using Weibull distribution, *Microwave Opt Technol Lett* 55 (2013), 1355–1358.
6. S. Weiqiang, RCS characterization of stealth target using chi-square distribution and lognormal distribution, *Progr Electromagn Res M* 27 (2012), 1–10.

7. A.M. Webb, Gamma mixture models for target recognition, *J Pattern Recogn* 33 (2000), 2045–2054.
8. A.G. Stove, Linear FMCW radar techniques, *IEE Proc F* 139 (1992), 343–350.
9. Y.-Q. Zhuang, Accurate statistical modeling method or dynamic RCS, *Progress in Electromagnetics Research Symposium Proceedings*, Guangzhou, China, August 2014, pp. 25–28.
10. A.D. Oliver, FMCW radar for hidden object detection, *IEE Proc* 135 (1988), 354–361.
11. C.M. Bishop, *Pattern recognition and machine learning*, Springer, New York, NY, 2006.

© 2016 Wiley Periodicals, Inc.

CMOS INTEGRATED LOW TX NOISE DIGITAL TRANSMITTER WITH TUNABLE DIRECTIONAL COUPLER FOR HIGH PERFORMANCE UHF RFID READER

Ying Guo, Yongan Zheng, Tao Xia, Xiucheng Hao, Le Ye, Xing Zhang, and Huailin Liao

Institute of Microelectronics, Peking University, Beijing 100871, China; Corresponding author: liaohl@pku.edu.cn

Received 11 November 2015

ABSTRACT: A fully CMOS integrated low TX noise UHF RFID digital transmitter with tunable directional coupler is proposed. The transmitter decreases the AM noise density to -144.6 dBc/Hz at 10 kHz offset by eliminating noisy conventional analog components and optimizing LO chain. The tunable transformer-based directional coupler which is feasible for CMOS integration exhibits high isolation performance of -55 dB over the entire band. The transmitter with quadrature DPA structure supports DSB/SSB/PR-ASK modulation, and with the directional coupler, it achieves 22.8 dBm peak power with drain efficiency of 37.8%. © 2016 Wiley Periodicals, Inc. *Microwave Opt Technol Lett* 58:1750–1756, 2016; View this article online at wileyonlinelibrary.com. DOI 10.1002/mop.29900

Key words: : UHF RFID; CMOS digital transmitter; CMOS directional coupler; TX noise; self-correlation

1. INTRODUCTION

RFID operating in the UHF band from 840 to 960 MHz is a remote autoidentification technology characterizing long recognition range, anticollision characteristics, high data rate, and small antenna size compared to barcode and near-field inductive coupled RFID system. Nowadays, Internet of Things (IoT) which is a huge network has been expanding its application scenarios rapidly with a dramatic market growth. Based on the technical features, UHF RFID technology is addressed to be one of the most important parts of IoT infrastructure. In IoT-oriented RFID network, an ultra-remote reading range up to 50 m in open air will lead to the emergence of many applications such as smart home, smart city, long distance vehicle identification, large warehouse management, etc. Besides, UHF RFID reader, which plays a communication node in IoT network is evolving towards high integration, low cost, and low power for application diversified requirement. It is a competitive way to integrate a large portion of a RFID reader in CMOS technology, including a power amplifier and a directional coupler.

Reader transmitter (TX) leakage noise is the most serious issue that limits the reading range. Different from other wireless communication systems, UHF RFID reader in nature is a miniature radar system, which transmits and receives signals at the

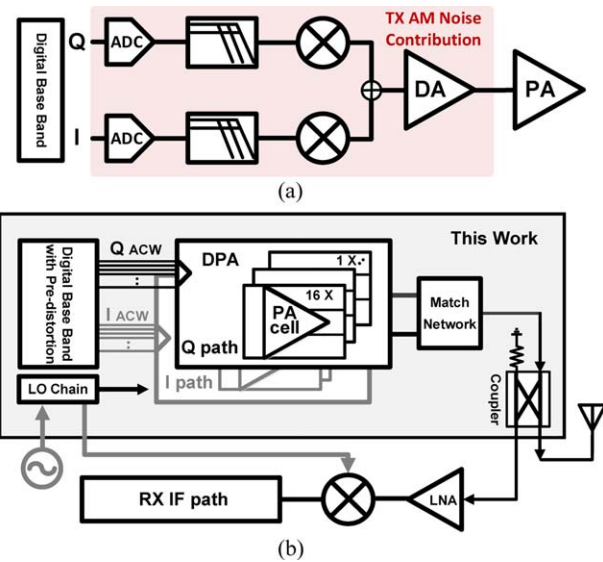


Figure 1 (a) Conventional UHF RFID reader transmitter. (b) Proposed UHF RFID reader system with low TX noise digital quadrature transmitter. [Color figure can be viewed in the online issue, which is available at wileyonlinelibrary.com]

same frequency. Due to the limited performance of couplers, RX sensitivity will be deteriorated dramatically by leakage noise, which includes phase noise and amplitude modulated (AM) noise caused by random phase and amplitude perturbation, respectively. The phase noise of leakage is usually cancelled to a large extent by self-correlation using the same LO for both TX path and RX path [1–5], but only correlated phase noise between LO signal and the leakage signal can be cancelled. TX AM noise that cannot be cancelled by correlation is produced mainly by the analog baseband, up-mixer, and PA driver in conventional systems as shown in Figure 1(a). Readers implemented in SiGe BiCMOS [1] could achieve a low TX noise. In Refs. 2 to 6, CMOS reader transmitters have been reported, but the AM noise of conventional TX architecture is still the reading range limitation. In our previous work [3], enlarging equivalent input magnitude of continuous wave (CW) signals in baseband is

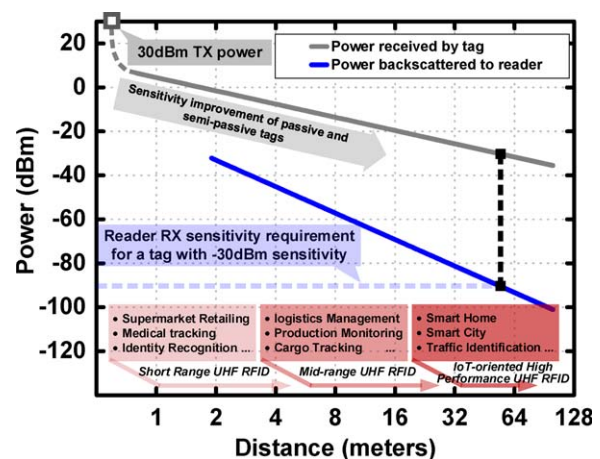


Figure 2 Forward and return link budgets in RFID system with the improvement of tag sensitivity. A reader TX power of 30 dBm, reader antenna gain of 6 dBi, tag antenna gain of 2 dBi, polarization mismatch loss of 2 Db are assumed. [Color figure can be viewed in the online issue, which is available at wileyonlinelibrary.com]